12th IFAC International Symposium on
Advanced Control of Chemical Processes
July 14-17, 2024. Toronto, Canada

A simple constraint-switching control structure for flexible operation of an alkaline water electrolyzer

Lucas Cammann, Johannes Jäschke

Department of Chemical Engineering, Norwegian University of Science and Technology Trondheim, NO-7491 (e-mail: lucas.cammann@ntnu.no, johannes.jaeschke@ntnu.no).

Abstract: Alkaline water electrolysis fueled by green electricity offers the promise of generating low-emission hydrogen for the envisioned energy transition. Coupling alkaline electrolysis processes to intermittent power supplies is however nontrivial, as the potential formation of explosive gas mixtures imposes strict purity requirements. This is especially crucial in low load scenarios, where gas production rates are low and foreign gas contamination can no longer be neglected. In this work we present a control structure for a stand-alone electrolysis unit which facilitates economically optimal operation under consideration of such safety constraints using only standard control elements. The proposed structure combines both objectives in the fast-acting regulatory control layer, alleviating the need for a supervisory real-time optimization layer. The performance of the control structure is attested through dynamic simulations of three different load scenarios.

Keywords: Plantwide control, Alkaline electrolysis, Economically optimal operation

1. INTRODUCTION

Alkaline electrolysis (AEL) is considered a viable option for the large-scale implementation of green hydrogen production due to its high technological maturity, low cost and availability (Buttler and Spliethoff, 2018). However, AEL processes are slower in ramp-up and shut-down than polymer-electrolyte membrane (PEM) electrolysis processes, making their coupling to intermittent power supplies more challenging. One reason for this lies in the requirement for tightly balanced pressure operation. This shall keep the permeation of electrolyte and therein dissolved gases across the membrane low to prohibit the creation of explosive gas mixtures (Schalenbach et al., 2016). This becomes particularly important in low load scenarios where the gas production rate is small compared to the transport mechanisms responsible for cross contamination, those being lye recirculation and permeation across the membrane.

To contain the foreign gas contamination, Qi et al. (2021) proposed and implemented a model predictive controller and an optimal curve tracking controller as pressure controller of the process. David et al. (2021) proposed a $\mathcal{H}_\infty$ optimal controller, controlling both the pressure and the difference between the liquid levels of the gas-liquid separators. More recently, Li et al. (2022) showed that by using both the lye flowrate and the pressure to control the gas contamination, the partial load range could be reduced from 11.78 % to 8.95 % in an experimental setup. While these previous works focused on improving gas purity control, the integration of the proposed solutions to the entire control system and its economic performance remains unclear. On the other hand, plantwide control structures as proposed recently by Shi et al. (2023) do not account for the restrictions imposed by gas purity control. This work aims at closing this gap by systematically developing a control structure for a stand-alone electrolyzer that is simple, yet safe and economically close to optimal for varying power inputs.

The contributions of this paper are then as follows. Firstly, the economically optimal operation of the electrolyzer is identified and partitioned into active constraint regions subject to an external power source. Here, each active constraint region represents a power range in which a unique set of inputs and outputs are optimally at their bounds. We present these regions and interpret them in terms of the resulting control requirements. Following that, a control structure based on the plantwide control procedure of Skogestad (2004) is presented. We show that this structure achieves steady state optimal performance when subjected to disturbed power inputs changing the optimal operating point. Importantly, this is achieved without the need for external setpoint updates by using selector blocks for reconfiguration of the control loops. We furthermore show that the proposed control structure gives safe transient operation. In short, we present a novel control structure for an alkaline water electrolyzer which facilitates optimal and safe operation and which can be implemented using only standard control elements.

To present these contributions, the remainder of the work is structured as follows. Following the introduction, a brief overview of the process as well as relevant operational constraints is given in Sec. 2. Building on that, the methodology of the control structure development and its implementation are presented in Sec. 3. Dynamic simulations of the proposed control structure showcase its performance in Sec. 4, with conclusions and recommendations given in Sec. 5.

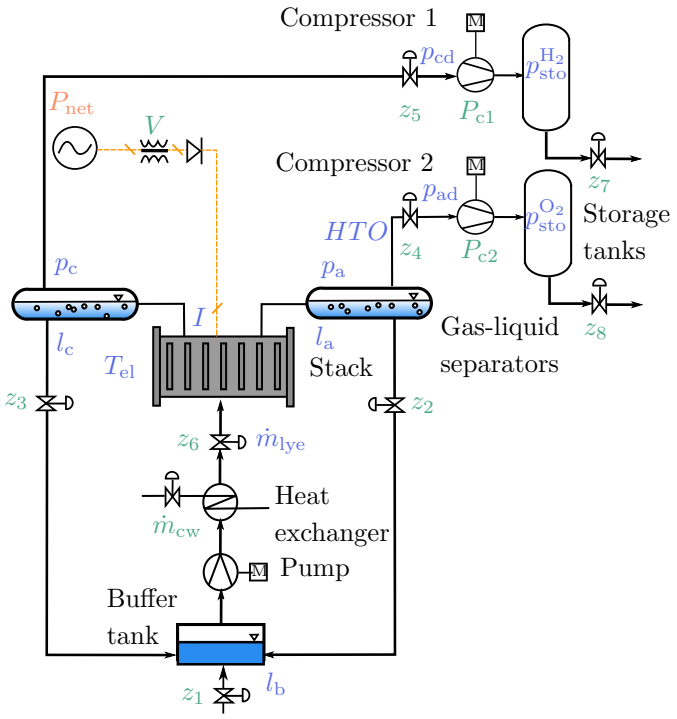

Fig. 1. Flowsheet of the considered electrolyzer, with inputs **u** highlighted in green, outputs **y** in blue and the disturbance **d** in orange.

2. PROCESS DESCRIPTION

The alkaline electrolysis process is based on the dynamic version of the model presented by Cammann and Jäschke (2023). The corresponding flowsheet can be seen in Fig. 1, in which the available inputs **u**, measurements **y** and the disturbance **d** are highlighted in blue, green and orange respectively. The applied voltage V influences the current density I in the stack, facilitating the following overall electrochemical reaction:

$$\mathrm{H_2O}(l) \rightarrow \mathrm{H_2}(g) + \frac{1}{2}\mathrm{O_2}(g), \tag{1}$$

with hydrogen being produced at the cathode and oxygen at the anode. The effluent gases are separated from the liquid lye (30 wt. % KOH) by means of gravity in two gas-liquid separators. At high pressures, more gas remains dissolved in the lye and is recirculated to the electrolyzer. Outgoing flows of gas and liquid are manipulated by the valves z_5 and z_3 at the cathodic side, and z_4 and z_2 at the anodic side. The liquid streams are mixed in the buffer tank, where additional water is supplied to the process to replenish water consumed by the electrolysis reaction. This external flow is manipulated through the valve z_1. The lye stream exiting the buffer tank is cooled in a heat exchanger, which is the only heat sink of the process other than heat losses to the surroundings. The lye flowrate $\dot{m}_{\mathrm{lye}}$ into the electrolyzer is manipulated through the valve z_6 located behind the heat exchanger. Not only does the lye flowrate serve the purpose of supplying the reactant to the electrolyzer and cooling it, it also affects the bubble coverage at the electrodes. Gas streams exiting the anodic and cathodic separators are compressed to the pressures in the respective storage tanks, from which gas is relieved through the valves z_7 and z_8.

2.1 Operational constraints

Certain constraints have to be satisfied at all times to ensure safe operation. Firstly, the foreign gas concentrations of hydrogen and oxygen respectively must to be contained in certain bounds to prevent the formation of explosive gas mixtures. The lower explosion limit of hydrogen in oxygen is ≈ 4 %, so the safety limit is set to half of this value, i.e. 2 % (Haug et al., 2017). Importantly, this value is only considered at the anode side. Going forward, the *HTO* ratio is defined as

$$HTO = \frac{x^{\mathrm{an}}_{\mathrm{H2}}}{x^{\mathrm{an}}_{\mathrm{O2}}}, \tag{2}$$

where x_{i} is the molar fraction of species i. A related limitation in the operation of alkaline electrolyzers is the requirement for balanced pressures on the anode and cathode to avoid strong cross-permeation of gases between the compartments. Schalenbach et al. (2016) state that the pressure driven permeation flux is approximately equal to the diffusive flux for pressure differences of 1 % magnitude of the absolute pressure. In this work, the maximal pressure of the electrolyzer is set to 15 bar, so a limit in the differential pressure Δp of 0.15 bar is imposed to contain pressure driven permeation. Lastly, alkaline electrolyzers are typically operated in the range of 50 °C to 80 °C. Higher temperatures increase the electrical efficiency, but also the risk of corrosion. Hence, the typically stated maximal temperature is also used in this work.

3. METHODOLOGY

The following section presents the development and implementation of the proposed control structure. For this purpose, an overview of the applied methodology and its results is followed by a description of the controller tunings and the numerical implementation.

3.1 Control structure development

The control structure is designed based on the "Top-Down" section of Skogestads plantwide control procedure (Skogestad, 2004).

(1) Define operational objective (cost) and constraints
(2) Identify degrees of freedom and optimize operation for disturbances
(3) Implement optimal operation
(4) Choose where to set production rate

In the following, the above steps are presented mainly in the given order. For the sake of brevity, related points are summarized and briefly explained.

Steps 1 + 2: Steady state optimization The economic objective is to maximize the hydrogen production rate given an external power input P_{net}. It is herein assumed that this power input is a measured disturbance **d**, and that the electrolyzer and the balance of plant are equally supplied by the external power source

$$P_{\mathrm{net}} = P_{\mathrm{e}} + \sum P_{\mathrm{c}} + P_{\mathrm{p}}. \tag{3}$$

The subscripts e, c and p herein denote the electrolyzer, compressor and pump respectively. For regularization, liquid levels are constrained and a minimal pressure drop

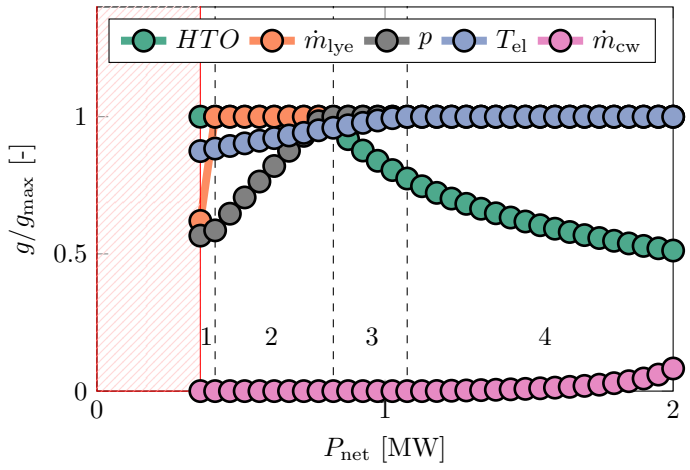

Fig. 2. Active constraint regions of selected variables for the steady state optimization.

across the valves of 1 bar imposed. The optimization problem is then formulated as

$$\begin{aligned} \max_{\mathbf{u}} \quad & \dot{n}_{\mathrm{H_2,out}} \qquad (4)\\ \text{s.t.} \quad & f(\mathbf{x},\mathbf{u},\mathbf{d}) = 0 \\ & HTO \leq 2\,\% \\ & 10\,^{\circ}\mathrm{C} \leq T_{\mathrm{el}} \leq 80\,^{\circ}\mathrm{C} \\ & 0.5\,\mathrm{kg\,s^{-1}} \leq \dot{m}_{\mathrm{lye}} \leq 15\,\mathrm{kg\,s^{-1}} \\ & 7.5\,\mathrm{bar} \leq p \leq 15\,\mathrm{bar} \\ & u_{\min} \leq \mathbf{u} \leq u_{\max}. \end{aligned}$$

Here, $f(\mathbf{x},\mathbf{u},\mathbf{d})$ entails our model equations, as well as the requirement outlined in Eq. 3. The remaining inequality constraints are imposed on safety critical variables, as well as on the inputs themselves. For the purpose of formulating the optimization problem, all inputs $\mathbf{u}$ are considered degrees of freedom. The nonlinear program of Eq. 4 is solved for 40 realizations of the power disturbance ranging from 0 to 2 MW. Fig. 2 shows the resulting optimal operating points of a selected number of constrained variables, scaled by their respective upper bound $g_{\max}$. Based on these variables four different operating regions can be identified, with the region from 0 kW to 350 kW being inoperable due to infeasibilities of the *HTO* constraint. The operable regions are defined as a power range in which a unique set of variables lies at their constraint and are numbered in Fig. 2, while the impermissible region is marked by a shaded red box. In the first two operable regions, the *HTO* is an active constraint at its upper bound and the cooling water flowrate at its lower bound. The results suggest that in this low power region operating with a high lye flowrate should be prioritized over operating at high pressures. Only at very low loads, i.e. in region 1, should the lye flowrate also be reduced to remain within *HTO* ratio safety limits. The third region is marked by the *HTO* ratio no longer being at its constraint, and instead both the lye flowrate and the anodic pressure assuming their maximal value. In this region, current densities are high enough to mitigate the influence of cross-contamination mechanisms. Lastly region 4 is defined by the electroyzer temperature reaching its upper constraint, at which point the cooling water has to gradually increase to keep the temperature at its bound.

Table 1. Overview of the switching logic between the identified regions.

Regions	Switch	Comment
$1 \rightarrow 2$	MV-MV	$\dot{m}_{\mathrm{lye}}$ shall saturate before p_{a}
$2 \rightarrow 3$	MV-CV	Control of *HTO* can be given up
$3 \rightarrow 4$	MV-CV	T_{el} reaches constraint

Steps 3 + 4: Implementation of optimal operation and throughput manipulator The optimal operation is fully constrained in all regions, meaning that all inputs to the system are at their respective constraint or controlling a CV at its constraint. This also means that optimal operation can be achieved by means of a switching logic. In regions 1 and 2, the *HTO* is an active constraint and has to be controlled to its limiting value. Since the current density is not available as manipulated variable, this leaves the lye flowrate and the anode side pressure as candidate manipulated variables, as proposed recently by Li et al. (2022). The results of the steady state optimization further confirm this, and additionally suggest a prioritization in which the lye flowrate is used as MV until saturation before using the anodic pressure. This MV-MV switching is facilitated as proposed by Skogestad (2023), who suggests to use two separate controllers (CC1 and CC2) with different setpoints instead of one split-range controller. This allows the respective controllers to be differently tuned and have separate anti-windup tracking. Both the lye flowrate and the anodic pressure are optimally kept at their upper bound when permitted by the *HTO* level, and it is chosen to supply the setpoints to these controllers through a `min`-selector. This facilitates the switch between regions 2 and 3, and supplying a higher setpoint to the concentration controller manipulating the lye flowrate ensures the correct saturation ordering between regions 1 and 2. From region 3 to 4, a MV-CV switching is necessary since the cooling water flowrate has to be used to ensure the electrolyzer temperature remains within bounds. An overview of the resulting switching logic can be found in Table 1. Lastly, the anodic and cathodic pressures have to be tightly balanced. While this is easily realizable under steady state conditions, it poses significant restrictions for the transient operation under changing loads. One straightforward way of relating these pressures is through a ratio controller. For the implementation at hand, the pressure of the anode side is of higher priority than that on the cathode side, as it directly relates to the safety critical *HTO* ratio. Hence, the pressure at the anode side is forwarded as setpoint to the pressure controller pC2 at the cathode side.

The main throughput manipulator (TPM) of the process is the applied voltage. It is necessary to control one flowrate within the lye recycle loop, which is achieved by pairing z_6 with the stream entering the electrolyzer. The resulting flow controller FC is hence a second TPM for the process. Regulatory control for the process is then achieved by controlling liquid and gas inventories according to the radiation rule around the TPMs. The inventory setpoints for the liquid levels and the storage pressures are invariant to the power input and do not have to be updated. The setpoints of the pressure controllers pC3 and pC4 are set to the anode and cathode side pressures, subtracted by a pressure drop Δp_{v} of 1 bar. The resulting plantwide control structure can be seen in Fig. 3.

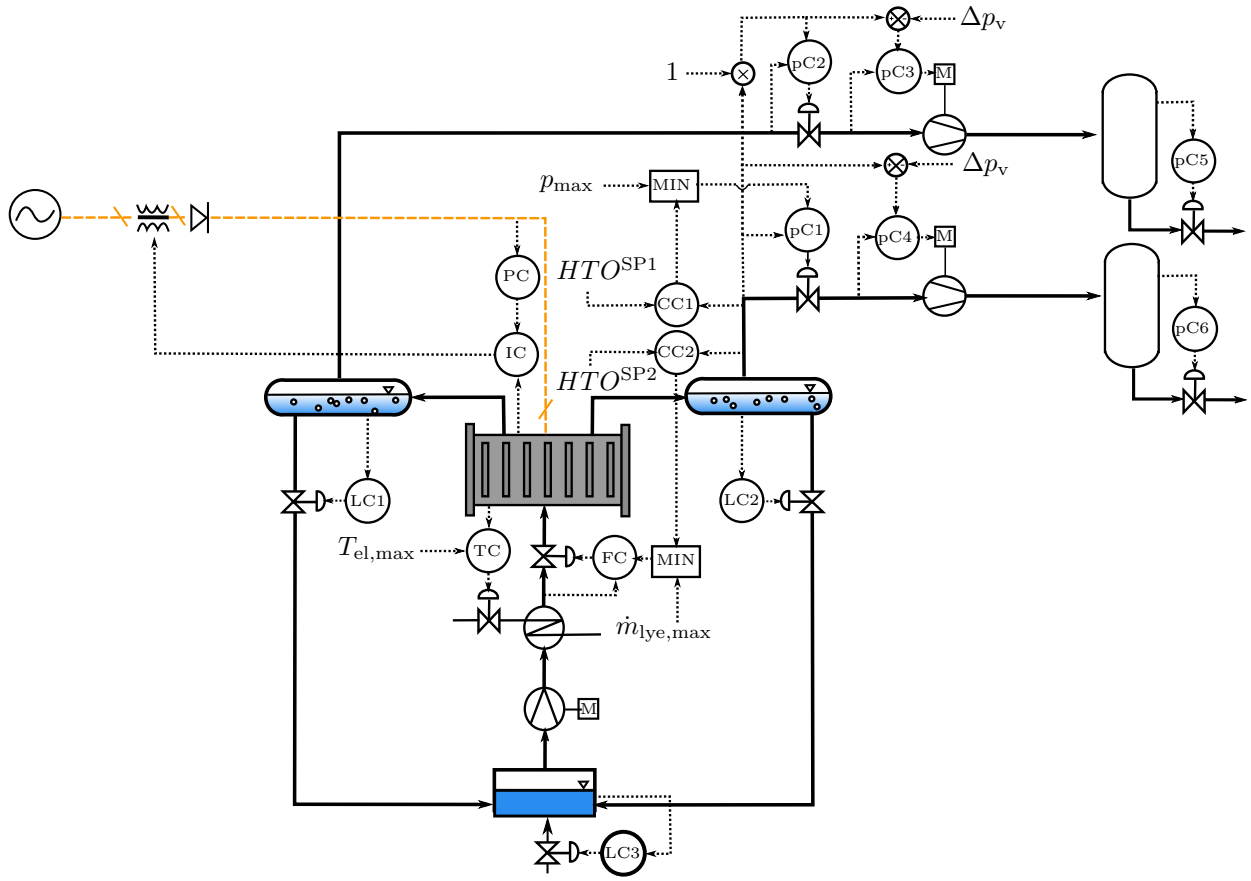

Fig. 3. Flowsheet of the electrolyzer plant with the developed control structure.

Controller tuning All controllers are tuned according to the SIMC rules for PI controllers (Skogestad, 2003), with step responses obtained by a 5 % step in the nominal input at an input power of 1 MW. For fast and robust control, the closed-loop time constant τ_c is chosen to be equal to the time delay θ throughout. An exception is the control of the anodic pressure, which is related to the control of the cathodic pressure according to

$$\tau_{pC1} = 3 \times \tau_{pC2}. \tag{5}$$

This is done to ensure the control of the cathode side pressure is sufficiently fast to follow the anode side pressure, which itself is controlled by the concentration controller CC1 at low loads. Anti-windup tracking is enabled for all controllers following Åström and Hägglund (2006), with the tracking time constant set equal to the integral time constant.

3.2 Numerical Implementation

The steady state optimization problem in Eq. 4 is solved using the interior point solver IPOPT (Wächter and Biegler, 2005), interfaced through the Julia package JuMP (Lubin et al., 2023). The dynamic Differential-Algebraic-Equation model is solved with a L-Stable Rosenbrock-W method after structural simplification using the ModelingToolkit package of Julia (Ma et al., 2021). Absolute and relative tolerances are both set to 10^{-10}.

4. SIMULATION RESULTS

In the following section dynamic simulation results of the control structure are presented. The response of safety critical variables, as well as the hydrogen production rate is analyzed for two load changes in the time span of 12 hours. Here, the power drops from 1 MW to 0.6 MW after 2 hours and then steps up to 1.6 MW after 10 hours. These load changes are deemed representative of the most extreme cases that can be encountered in terms of ramp-up and ramp-down. Furthermore, they represent a switching of active constraints from regions 3 → 2 → 4. To further assess the economic performance, a comparison is drawn between the hydrogen production rate and the production rates computed in the steady state optimization.

4.1 Operational constraints

Pressure difference Fig. 4 shows the pressure difference between the anodic and cathodic side of the electrolyzer, together with the minimal and maximal bounds outlined in Sec. 2.1. Fig. 4 also shows a close-up of the transient response in the first ten minutes after the step at 2 h, as well as an indication of the current constraint region. It can be seen that the pressure difference is well contained within the bounds by pC2, even in transient operation. These transients occur instantaneously with the changes in the applied power at 2 h and 10 h, as the change in current density translates to a change in gas production at the cathode and anode side. Since twice the amount of moles is produced at the cathode than the anode, rate

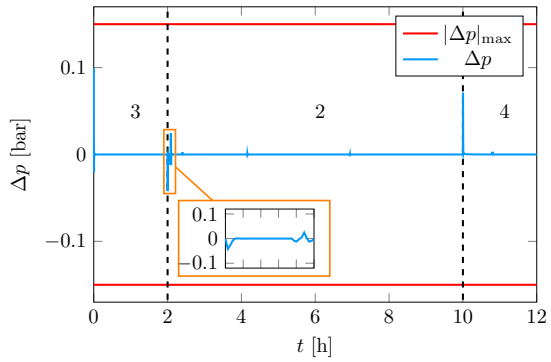

Fig. 4. Anodic and cathodic pressure difference for given load changes.

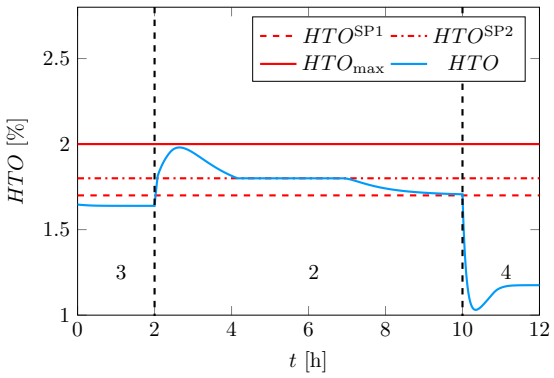

(a) *HTO*

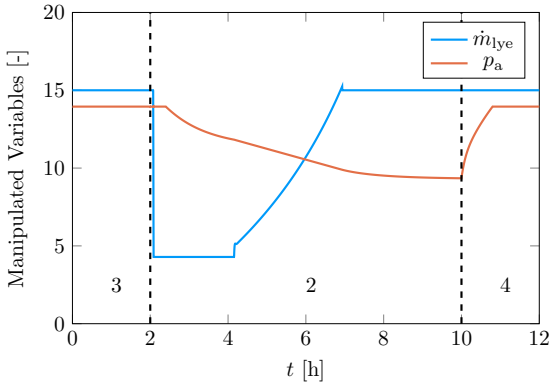

(b) Manipulated variables of *HTO* controllers

Fig. 5. *HTO (a)*, and manipulated variables of the concentration controllers *(b)* for given load changes.

changes will inevitably lead to pressure differences without feedforward information. The close-up in Fig. 4 further shows a second, later spike after the first power step. This is due to a reduction in lye flowrate, as will be seen below.

HTO ratio Fig. 5a shows the response of the *HTO* to the set load changes, while Fig. 5b shows the response of the lye flowrate and the anodic pressure used as manipulated variables by the concentration controllers. In both plots, the respective operating regions, as well as the setpoints of the concentration controllers are clearly marked. It can be seen that the *HTO* constraint is not breached at any point of operation. As the power drops at 2 h the *HTO* rises instantaneously, triggering a response of both concentration controllers. Conceivably, the response in the lye flowrate

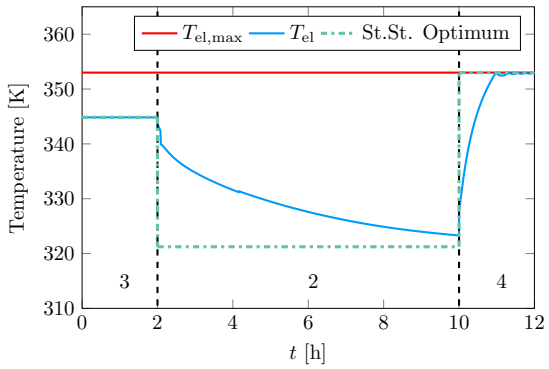

Fig. 6. Electrolyzer temperature for given load changes.

is faster, and CC2 drives the *HTO* to its setpoint of 1.8%. Simultaneously, the pressure in the system is further reduced as CC1 drives the *HTO* to its lower setpoint. This in turn leads to a "reset" of the lye flowrate to its upper constraint, in line with the prioritization found in the steady state optimization for region 2. As the applied power increases at 10 h, control of the *HTO* can be given up and also the pressure resets to its upper constraint.

Temperature Fig. 6 shows the dynamic temperature response together with the setpoint of TC and the steady state optimal value. For the first 2 hours, the electrolyzer is operated in region 2 where the losses in the electrolyzer are too low to sustain the temperature at its upper constraint. Loss related heat production is further reduced as the power drops at 2 h, leading to a steady decrease in temperature. Since the temperature is not actively controlled in region 2 this decline is rather slow, as can be seen by the fact that the steady state optimal temperature is not reached by the 10 h mark. As will be argued below, loss of control in this region is actually beneficial from an economic point of view. Tight control of the temperature at its upper constrain is reestablished shortly after the 10 h mark, where the step in the applied power leads to a rapid increase in temperature.

4.2 Optimality

Fig. 7 shows the hydrogen production rate achieved by the control structure together with the steady state optimal values at the respective power levels. In all regions, the presented scheme controls the system to its steady state optimum without the need for setpoint updates. During the ramp-down from region 3 $\rightarrow$ 2 the production rate is initially below its optimal value and increases above it as time progresses. The reason for the later increase in region 2 lies, perhaps counter intuitively, in the loss of control of the electrolyzer temperature at low power inputs. As was seen in Sec. 4.1.3, this circumstance leads to the temperature only gradually decreasing when the power is reduced. These elevated electrolyzer temperatures lead to a higher efficiency in the electrolyzer and allow for a quicker ramp-up to higher power levels. The initial losses are then attributed to transient reductions of the lye recirculation.

5. CONCLUSIONS AND RECOMMENDATIONS

This work shows the systematic development of a simple constraint-switching control structure for a stand-alone

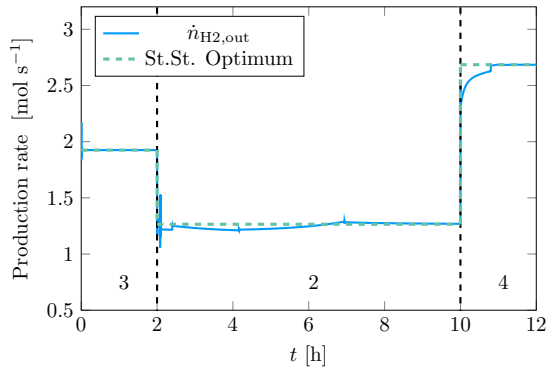

Fig. 7. Comparison of prodution rate and steady state optimal production rate for given load changes.

alkaline electrolyzer. The efficacy of the proposed control structure is demonstrated through dynamic simulations, where it is found that even extreme load changes are safely handled. It is further shown that the control structure controls the disturbed process to its new steady state optimum without the need for external setpoint updates.

The results of this work demonstrate that optimal performance for single alkaline water electrolyzer systems can be achieved by employing simple control elements. This offers several benefits over more computationally expensive control architectures, employing for example real-time optimization or model predictive control. As such, it is more easily scalable to systems consisting of several electrolyzers in terms of interpretability and computational complexity. Additionally, it is implemented in the fast-acting regulatory control layer based purely on feedback information. Not only does this enable fast disturbance rejection, but also alleviates the need for model and parameter updates in the face of electrolyzer and equipment degradation. Lastly, it is considered robust towards inaccuracies in the offline optimization model as long as the representation of the active constraint regions is qualitatively correct.

However, further challenges need to be addressed on the quest towards flexible operation of alkaline electrolysis processes. Firstly, the herein investigated system consists of only a single electrolyzer and does not capture the added complexities of operating multiple electrolysis stacks with high levels of system integration. Secondly, the economic optimization conducted in this work only considers steady state performance and cannot resolve any scheduling objectives. Both of these issues might warrant the use of more advanced control solutions. It is hence recommended to work further towards large-scale AEL system models, investigate their optimal dynamic operation and compare their performance given different control solutions.

ACKNOWLEDGEMENTS

The authors would like to thank Vidar Alstad and Anushka Perera for fruitful discussions.

REFERENCES

Åström, K. and Hägglund, T. (2006). *Advanced PID control*. ISA - The Instrumentation, Systems and Automation Society.

Buttler, A. and Spliethoff, H. (2018). Current status of water electrolysis for energy storage, grid balancing and sector coupling via power-to-gas and power-to-liquids: A review. *Renewable and Sustainable Energy Reviews*, 82, 2440–2454.

Cammann, L. and Jäschke, J. (2023). Comparing operational strategies for alkaline electrolysis systems considering a probabilistic wind power distribution. In A.C. Kokossis, M.C. Georgiadis, and E. Pistikopoulos (eds.), *33rd European Symposium on Computer Aided Process Engineering*, volume 52 of *Computer Aided Chemical Engineering*, 3147–3152. Elsevier.

David, M., Bianchi, F., Ocampo-Martinez, C., and Sánchez-Peña, R. (2021). H2 purity control of high-pressure alkaline electrolyzers. *IFAC-PapersOnLine*, 54(3), 109–114. 16th IFAC Symposium on Advanced Control of Chemical Processes ADCHEM 2021.

Haug, P., Koj, M., and Turek, T. (2017). Influence of process conditions on gas purity in alkaline water electrolysis. *International Journal of Hydrogen Energy*, 42(15), 9406–9418.

Li, Y., Zhang, T., Deng, X., Liu, B., Ma, J., Yang, F., and Ouyang, M. (2022). Active pressure and flow rate control of alkaline water electrolyzer based on wind power prediction and 100 % energy utilization in off-grid wind-hydrogen coupling system. *Applied Energy*, 328, 120172.

Lubin, M., Dowson, O., Dias Garcia, J., Huchette, J., Legat, B., and Vielma, J.P. (2023). JuMP 1.0: Recent improvements to a modeling language for mathematical optimization. *Mathematical Programming Computation*.

Ma, Y., Gowda, S., Anantharaman, R., Laughman, C., Shah, V., and Rackauckas, C. (2021). Modelingtoolkit: A composable graph transformation system for equation-based modeling.

Qi, R., Gao, X., Lin, J., Song, Y., Wang, J., Qiu, Y., and Liu, M. (2021). Pressure control strategy to extend the loading range of an alkaline electrolysis system. *International Journal of Hydrogen Energy*, 46(73), 35997–36011.

Schalenbach, M., Lueke, W., and Stolten, D. (2016). Hydrogen diffusivity and electrolyte permeability of the zirfon perl separator for alkaline water electrolysis. *Journal of The Electrochemical Society*, 163(14), F1480.

Shi, Y., Hu, X., Zhang, Z., Lu, S., Xie, L., and Su, H. (2023). Plant-wide modeling, design consideration, and practical hierarchical control strategy considering key variable integral characteristics for an industrial alkaline water electrolyzer plant. *Industrial & Engineering Chemistry Research*, 62(36), 14441–14455.

Skogestad, S. (2003). Simple analytic rules for model reduction and PID controller tuning. *Journal of Process Control*, 13(4), 291–309.

Skogestad, S. (2004). Control structure design for complete chemical plants. *Computers Chemical Engineering*, 28(1), 219–234. Escape 12.

Skogestad, S. (2023). Advanced control using decomposition and simple elements. *Annual Reviews in Control*, 56, 100903.

Wächter, A. and Biegler, L.T. (2005). On the implementation of an interior-point filter line-search algorithm for large-scale nonlinear programming. *Mathematical Programming*, 106(1), 25–57.